Fouling characteristics of internal helical-rib roughness tubes using low-velocity cooling tower water

Wei Li [a], Ralph L. Webb [b,*]

[a] *Engineered Air, 320580 W. 83rd St., Desoto, KS 66018, USA*
[b] *Department of Mechanical Engineering, The Pennsylvania State University, University Park, PA 16802, USA*

Abstract

This paper provides long-term cooling tower water fouling data in seven 15.54 mm I.D. copper, helically ribbed tubes taken at low water velocity (1.07 m/s). The ranges of geometric parameters were number of rib starts (18–45), helix angle (25–45°), and height (0.33–0.55 mm). These geometries provide a new class of internal enhancement that is typical of commercially enhanced tubes presently used in water chillers. There are two ranges of fouling characteristics based on internal dimensions: linear range and non-linear range. The ratio of the enhanced-to-plain tube fouling resistance linearly increases with increasing the product of area indexes and efficiency indexes in linear range and the linear relationship fails in non-linear range. A series of semi-theoretical fouling correlations as a function of the product of area indexes and efficiency indexes were developed. They were applicable to different internally ribbed geometries within the above dimensional range. A series of linear multiple regression correlations as a function of geometric variables and Reynold numbers were also developed. The average deviation of the two series of correlations was 4.4% and 4.8%, respectively. The correlations can be directly used to assess the fouling potential of enhanced tubes in actual cooling water situations. © 2002 Published by Elsevier Science Ltd.

Keywords: Fouling; Cooling tower; Enhanced tube; Turbulent flow

1. Introduction

Enhanced tubes have been widely used because of their superior heat transfer performance. Two primary categories of the internally enhanced tubes have been historically identified: "rough" tubes and "internally finned" tubes. A rough tube, with a small number of starts, provides enhancement by local boundary layer separation and reattachment between the ribs and small surface area increase. As the number of starts increases, the tubes provide significant surface area increases, which are characteristic of "internally finned" tubes. Traditional internally finned tubes typically have helix angles between 0° and 25° and the enhancement mech-

anism is associated with the area increase alone. Local flow separation is assumed not to occur in internally finned tubes having a small helix angle and large area increase. The seven enhanced tubes in this study are described as helical-rib roughened tubes. Hence, they cannot be described as either classic "rough" tubes or "internally finned" tubes. They probably provide some of the attributes of a rough tube (local flow separations) and some of an internally finned tube (large surface area increase). It is likely that the flow will tend to swirl, although it is expected that the swirl angle will be significantly less than the helix angle. Little understanding exists of the flow and enhancement mechanism of the seven tubes. It is probable that two basic types of flow can occur inside a ribbed tube enhanced with intermediate helix angles. The first is the rotational flow mainly caused by the helix angle of the ribs. The other type of flow is the flow separation. The momentum in the axial direction is much larger than the angular momentum caused by the ribs, which results in the fluid

---

* Corresponding author. Tel.: +1-814-865-0283; fax: +1-814-865-1344.
E-mail addresses: weili96@hotmail.com (W. Li), rlwebb@psu.edu (R.L. Webb).

Nomenclature

A_w	inside wetted surface area (m²)
A_c	cross-sectional area (m²)
C	constant to be determined experimentally (dimensionless)
c_p	specific heat of water (J/kg K)
D_i	internal tube diameter, or diameter to root of fins (m)
e	internal rib height (average value) (m)
f	fanning friction factor (dimensionless)
G	mass velocity $(= \dot{m}/A_c)$ (kg/m²)
j	Colburn j-factor $(= St\, Pr^{2/3})$ (dimensionless)
m	constant to be determined experimentally (dimensionless)
$\dot{m}$	mass flow rate (kg/s)
n_s	number of starts
P	axial element pitch (m)
ΔP	tube side pressure drop (N/m²)
Re	tube-side Reynolds number $(= D_i G/\mu)$ (dimensionless)
R_f	fouling resistance (m² K/W)

R_f°	fouling resistance at the end of one cooling season (m² K/W)
R_f^{*}	asymptotic fouling resistance (m² K/W)
Pr	Prandtl number (dimensionless)
St	Stanton number (h/Gc_p) (dimensionless)
t_t	fin tip thickness (m)
U	fluid velocity (m/s)

Greek symbols

α	helix angle (°)
β	area index, $(A_w/A_{wp})/(A_c/A_{cp})$ (dimensionless)
γ	included angle between sides of ribs (°)
ζ	the deposit bond strength (dimensionless)
η	efficiency index, $(j/j_p)/(f/f_p)$ (dimensionless)
ϕ_d	rate of deposition (m² K/W s)
τ_w	wall shear stress (N/m²)
μ	dynamic viscosity at bulk water temperature (kg/m s)

Subscripts

p	plain surface
pre	predicted
exp	experimental

separating at the ribs. One of the characteristics of this flow is the reattachment of the fluid to the surface between the ribs. An important design factor that controls this reattachment length is the ratio of rib pitch to height (p/e). Further, the space downstream of the rib to the reattachment point is characterized by recirculating zone. Reattachment does not occur when the pitch of roughness is reduced to less than approximately five rib heights, and the main flow is forced to ''glide over'' the ribs and a secondary flow is created between the ribs. Liu and Jensen [1] numerically modeled periodically fully developed, single-phase turbulent flow and heat transfer in two helical finned tubes. However, no flow visualization experiments or numerical simulations have been reported in the literature for these geometries.

Most work done on predictive fouling models have been directed at plain tubes. Morse and Knudsen [2] performed a series of fouling tests with simulated cooling tower water on the exterior of a smooth tube in an annulus. Taborek et al. [3] proposed a fouling model for plain tubes using river water in cooling tower systems with low content of suspended solids.

With respect to enhanced tubes, several investigators have performed accelerated particulate fouling in enhanced tubes, such as Kim and Webb [4] and Somerscales et al. [5]. Additionally, Chamra and Webb [6] proposed a model to predict long-term fouling using their accelerated particulate fouling model, but they did not have long-term data to evaluate their model. Watkinson [7] performed accelerated precipitation fouling tests on internally enhanced tubes.

Little information exists on long-term fouling in enhanced tubes. Rabas et al. [8] monitored the fouling characteristics of helically corrugated (indented) steam condenser tubes in an electric utility plant for 15 months. This condenser used the Wolverine Korodense-corrugated tube with river water operating at 1.25–2.75 m/s water velocity. Chapter 10 of Webb [9] summarizes much of the relevant prior work.

Webb and Li [10] described the experimental results of long-term fouling tests for cooling tower water flowing inside enhanced tubes. Fouling data were measured for the seven helical-rib roughened tubes for more than a 2500-h operating period. These tests were conducted over a full cooling season which is considered as ''long-term'' data. Based on the experimental results, Li [11] proposed a new concept – oscillatory asymptotic fouling model, which can be used for all categories of fouling and asymptotic fouling model is a special case of the new model. Li and Webb [12] further demonstrated that there is a unique relationship between the long-term fouling data in practical cooling tower water systems and accelerated particulate fouling data. This allows one to infer the relative long-term fouling performance of different enhanced tube geometries from accelerated particulate fouling data.

The purpose of this paper is to provide correlations of the experimental results of Webb and Li [10] to quantitatively define the effect of rib height, rib axial pitch, and helix angle on the tube fouling performance. These correlations have practical industrial application. This is the first work to report correlations that account

for the effect of the enhancement dimensions on long-term fouling of enhanced tubes in practical cooling tower systems.

2. Tube geometries and experimental method

The test geometries include seven enhanced copper tubes and a plain copper tube. Because the tube geometries and test procedures are fully described in Webb and Li [10], only brief description is given here. The geometry details are defined in Table 1. The geometries vary the number of starts (n_s), helix angle (α), and fin height (e). All fins were of a trapezoidal cross-section shape with a 41° included angle. One of the tubes (Tube 1) is a plain tube and is used to compare to the other seven tubes that have internal enhancement. All eight tubes have $D_i = 15.54$ mm (0.612 in.), and were made with 1024 fins/in (0.90 mm high) on the outer surface. The fouling mechanisms possible in a cooling tower water condenser may be precipitation fouling, biological fouling, corrosion fouling, and particulate fouling. In a practical sense, only two mechanisms were expected in the present tests – precipitation and particulate fouling. This is because the water was treated with corrosion inhibitors and biocides. These acted to inhibit corrosion and biological fouling. Precipitation fouling is expected in cooling tower systems. The heated water will precipitate $CaCO_3$ or $MgCO_3$ salts contained in the water. Particulate fouling is also expected, because of airborne dust exposed to the water in the cooling tower. Hence, the present interests are primarily limited to the combination of precipitation fouling and particulate fouling.

The fouling test condenser was connected in parallel with the condenser of an 880-kW (250-ton) water chiller in a six-story building on the Penn State University campus. The cooling tower water supplied to the main refrigerant condenser was also supplied to the tubes in the fouling condenser. It contains sixteen 3.66 m (12.0 ft) long tubes, installed as eight pairs of identical tubes (seven pairs of enhanced tubes and one pair of plain tube geometry). Reasoning for the pairs is to have one of the paired tubes run as an unfouled control and let the other tube experience long-term fouling. The unfouled condition was maintained through regular manual brushing. The tubes were horizontally paired to minimize local differences in condensing coefficient. At start of the season, all 16 tubes of the test condenser were manually brushed and an aqueous acidic solution was re-circulated to dissolve any calcium deposits not removed by the manual brushing. The fouling resistance was determined by taking the difference between the U-values of the fouled and "clean" tubes, as described by Webb and Li [10].

The present tests were conducted at the following operating conditions:

1. The cooling tower water was circulated through the condenser at 1.07 m/s (3.5 ft/s, $Re = 16,000$) tube side velocity in a one-pass arrangement. This is considered a low-velocity operating condition for a refrigerant condenser. It was chosen as a "worst case" condition.
2. The foulant water chemistry was 800 ppm ($\pm 20\%$) calcium hardness, 1600–1800 $\mu\Omega$ electrical resistance, and 8.5 pH. The water chemistry was measured was made every two weeks.
3. Typical operating conditions for the plain tube were 29.2 °C water inlet temperature was, 32.5 °C water outlet temperature, and 35.6 °C refrigerant condensing temperature. Water inlet and outlet temperatures were measured with thermistors in thermo-wells.

Foulant samples were removed after the study, and were chemically analyzed and reported in Li and Webb [12]. The analysis showed that 59% fouling deposit are calcium carbonate, caused by precipitation fouling. The remaining 40% are non-crystallizing particles including Silica (from sand particles in water), copper oxide (from copper tubing), iron phosphate/silicate (from iron piping), and aluminum silicate (from unidentified aluminum in the system). The analysis suggests that both precipitation and particulate fouling occurred.

Table 1 also shows experimental data: the ratio of the enhanced-to-plain tube heat transfer coefficients (clean

Table 1
Experimental fouling ratio and experimental heat transfer enhancement ratio (referred to plain tube) vs. tube geometries

Tube	R_f^*/R_{fp}^*	R_f°/R_{fp}°	η	β	n_s	e (mm)	α°	p/e	j/j_p
2	7.44	5.15	1.18	1.66	45	0.33	45	2.81	2.32
5	5.65	3.40	1.04	1.75	40	0.47	35	3.31	2.26
3	3.25	2.26	1.05	1.56	30	0.40	45	3.50	2.33
6	2.69	1.57	1.01	1.52	25	0.49	35	5.02	2.08
7	2.47	1.51	1.05	1.52	25	0.53	25	7.05	1.93
8	2.03	1.25	0.98	1.40	18	0.55	25	9.77	1.51
4	1.94	1.13	0.95	1.24	10	0.43	45	9.88	1.74
1.0	1.0	1.0	1.0	1.0	n/a	n/a	n/a	n/a	1.0

$D_i = 15.54$ mm, $\gamma = 41°$, $t_t = 0.024$ mm, $R_{fp}^* = 3.2E - 5$ m^2 K/W, $R_{fp}^\circ = 2.8E - 5$ m^2 K/W.
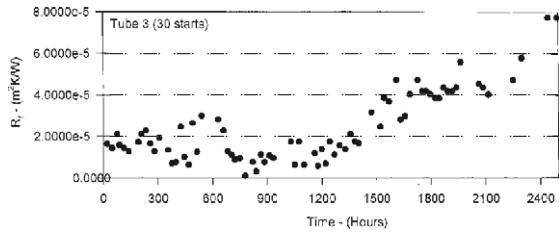
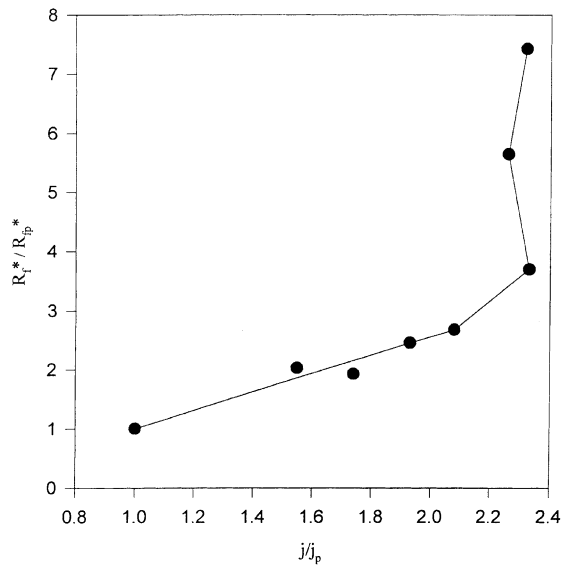Fig. 1. A sample of experimental fouling data.

Fig. 2. Experimental asymptotic fouling ratio vs. experimental heat transfer enhancement ratio, referred to plain tube.

tube data), the ratio of the enhanced-to-plain tube asymptotic fouling resistance and the ratio of the enhanced-to-plain tube fouling resistance at the end of one cooling season. Table 1 data are listed in order of decreasing fouling resistance. Fig. 1 shows a sample fouling data of a tested tube 3. Fouling data of the other tubes, and the fouling data deduction process were given in Webb and Li [10] and Li and Webb [12]. Fig. 2 shows the ratio of the enhanced-to-plain tube fouling resistance (R_f^*/R_{fp}^*) vs. the clean tube heat transfer enhancement ratio (h/h_p) in Table 1. The figure suggests a unique relationship between R_f^*/R_{fp}^* and h/h_p, which is related to the internal tube geometry.

3. Fouling data analysis

3.1. Heat-mass transfer analogy

Taborek et al. [3] has shown that the asymptotic fouling resistance can be written as

$$R_f^* \propto \frac{\xi \phi_d}{\tau_w},   (1)$$

where ξ is the deposit strength factor, ϕ_d is the removal rate. Watkinson [14] states that most applicable experimental results of scaling fouling in enhanced tubes have involved some particulate deposition. This is either organic material or water content. Watkinson made two assumptions in his model:

1. The ϕ_d/ϕ_{dp} ratio linearly increases with increasing j/j_p. This is confirmed in Fig. 2, which shows that the R_f^* ratio linearly increases with increasing j/j_p when $j/j_p < 2.26$.
2. The deposit strength factor (ξ) is the same for both plain tube and enhanced tubes. Taborek et al. [3] stated that ξ was affected by deposit structure, concentration and type of suspended solids, and by flow velocity.

Then, he obtained the following equation:

$$\frac{R_f^*}{R_{fp}^*} \propto \frac{j/j_p}{\tau_w/\tau_{wp}}.   (2a)$$

Eq. (2a) can be expressed as

$$\frac{R_f^*}{R_{fp}^*} = C\left(\frac{j/j_p}{\tau_w/\tau_{wp}}\right)^m,   (2b)$$

where C and m are the constants to be determined experimentally.

3.2. Formulation of the wall shear stress, τ_w

For a smooth surface, the wall shear stress is the only component that contributes to the friction. For rough surfaces, however, a fraction of the pressure drop is caused by profile drag on roughness elements. Because the $e/D_i < 0.04$ of the tubes investigated in this study is small, the momentum in the axial direction is much larger than the angular momentum promoted by the ribs. It is assumed that only the wall shear stress portion of the total friction contributes to the foulant removal process, i.e., profile drag by the roughness element does not contribute to the removal process. We use the apparent shear stress, obtained from pressure drop data, to approximate the wall shear stress (τ_w). The τ_w is given by

$$\Delta P A_c = \tau_w A_w,   (3)$$

where A_w is a wetted area, A_c is a cross-section area. Combining Eqs. (2b) and (3):

$$\frac{R_f^*}{R_{fp}^*} = C(\beta\eta)^m,   (4)$$

$\beta = (A_w/A_{wp})/(A_c/A_{cp})$ is an area index and $\eta = (j/j_p)/(f/f_p)$ is the efficiency index.

3.3. Fouling correlation

Table 1 lists the fouling factor ratio R_f°/R_{fp}° at the end of the cooling season and the asymptotic fouling factor ratio R_f^*/R_{fp}^*. We have previously noted that the water velocity is about half that used in typical condenser applications. Rabas et al. [8] and Lee and Cho [15] showed that fouling of condenser cooling tower water has asymptotic behavior in enhanced-tube and plain tube heat exchangers. Li and Webb [12] did curve-fitting of the data points R_f° to obtain the asymptotic fouling resistance R_f^*. By comparing the asymptotic fouling resistance between accelerated particulate fouling and long-term cooling tower water fouling, Li and Webb [12] successfully proved that there is an analogy between them, both for plain and enhanced tubes. Table 1 shows that $R_f^\circ < R_f^*$, which means that the asymptotic value was not attained at the end of the cooling season. By correlating R_f°/R_{fp}° and R_f^*/R_{fp}^* with $\beta\eta$ in Table 1, we obtained the following correlations:

$$\frac{R_f^\circ}{R_{fp}^\circ} = \beta\eta, \quad 10.0 > p/e \geqslant 5.0, \tag{5a}$$

$$\frac{R_f^\circ}{R_{fp}^\circ} = 0.178(\beta\eta)^{5.03}, \quad p/e < 5.0, \tag{5b}$$

Eqs. (5a) and (5b) have an average deviation of 4.5%.

$$\frac{R_f^*}{R_{fp}^*} = 1.59\beta\eta, \quad 10.0 > p/e \geqslant 5.0, \tag{6a}$$

$$\frac{R_f^*}{R_{fp}^*} = 0.36(\beta\eta)^{4.55}, \quad p/e < 5.0. \tag{6b}$$

Eqs. (6a) and (6b) have an average deviation of 4.3%. The average of deviation of all the four correlations is 4.4%. The semi-theoretical correlations are applicable to different internally ribbed geometries within the dimensional range of those tested. The correlations predicted $(R_f^*/R_{fp}^*)_{pre}/(R_f^*/R_{fp}^*)_{exp}$ and $(R_f^\circ/R_{fp}^\circ)_{pre}/(R_f^\circ/R_{fp}^\circ)_{exp}$ within 10% as shown in Fig. 4.

3.4. Linear multiple regression correlations

Webb et al. [13] developed linear multiple regression correlations to predict the clean tube j and f factors for the seven enhanced tubes in Table 1. Their correlations are:

$$f = 0.108Re^{-0.283}n_s^{0.221}(e/D_i)^{0.785}\alpha^{0.78}, \tag{7}$$

$$j = 0.00933Re^{-0.181}n_s^{0.285}(e/D_i)^{0.323}\alpha^{0.505}. \tag{8}$$

The correlations show that both f and j increase with increasing n_s, e/D_i, and α. However, f is a stronger function of e/D_i and α than is j. Conversely, f is a weaker function of n_s than is j. The average deviations of the friction and heat transfer correlations are 4.9%

and 3.8%, respectively. The correlations over-predicted the friction factor 0–15% and predicted the j-factor within 10%. The measured plain tube friction factor agrees well with the Blasius friction factor ($f_p = 0.316Re^{-0.25}$). The experimental j-factor is also agrees very well with that given by the Seider-Tate (1936) equation ($j_p = 0.027Re^{-0.2}$). Therefore, the efficiency index $[\eta = (j/j_p)/(f/f_p)]$ is

$$\eta_{pre} = 0.13Re^{0.052}n_s^{0.06}(e/D_i)^{-0.462}\alpha^{-0.05}. \tag{9}$$

Eq. (9) has an average deviation of 1.85% from the experimental η-values in Table 1.

By correlating R_f°/R_{fp}° and R_f^*/R_{fp}^* with $\beta\eta_{pre}$, we obtained the following correlations:

$$\frac{R_f^\circ}{R_{fp}^\circ} = \beta\eta_{pre}, \quad 10.0 > p/e \geqslant 5.0, \tag{10a}$$

$$\frac{R_f^\circ}{R_{fp}^\circ} = 0.187(\beta\eta_{pre})^{4.93}, \quad p/e < 5.0. \tag{10b}$$

Eqs. (10a) and (10b) have an average deviation of 4.5%.

$$\frac{R_f^*}{R_{fp}^*} = 1.59\beta\eta_{pre}, \quad 10.0 > p/e \geqslant 5.0, \tag{11a}$$

$$\frac{R_f^*}{R_{fp}^*} = 0.392(\beta\eta_{pre})^{4.4}, \quad p/e < 5.0. \tag{11b}$$

Eqs. (11a) and (11b) has an average deviation of 5.1%. The average of deviation of all the four correlations is 4.8%. The linear multiple regression correlations are valid for the following range of dimensions for any enhanced tube inside diameter: $0.024 \leqslant e/D \leqslant 0.041$, $2.81 \leqslant p/e \leqslant 9.88$, $25 \leqslant \alpha \leqslant 45°$, $\gamma = 41°$, $t_t/D_i = 0.015$. Fig. 3 summarizes the correlations (5), (6), (10), and (11) by showing the fouling resistance ratios (enhanced-to-plain tube) versus number of rib starts. Fig. 4 is an error plot showing $(R_f^*/R_{fp}^*)_{pre}/(R_f^*/R_{fp}^*)_{exp}$ and $(R_f^\circ/R_{fp}^\circ)_{pre}/(R_f^\circ/R_{fp}^\circ)_{exp}$ for the four correlations. The correlations predicted $(R_f^*/R_{fp}^*)_{pre}/(R_f^*/R_{fp}^*)_{exp}$ and $(R_f^\circ/R_{fp}^\circ)_{pre}/(R_f^\circ/R_{fp}^\circ)_{exp}$ within 13%.

It is interesting to compare the R_f^* ratios (enhanced-to-plain tube) with the j/j_p ratios, which are shown in Fig. 2. There are clearly two ranges. A linear range exists for tubes 6, 7, 8, and 4, which have $p/e \geqslant 5.0$, and $j/j_p < 2.26$. In this linear range, the R_f^* ratio linearly increases with increasing j/j_p, which supports the apparent shear stress assumption, and is in agreement with the first previously stated assumption of Watkinson's [14]. Linearity can be established only when all the three assumptions are valid. The R_f^* ratio shows non-linear relationship behavior for tubes 2, 3, and 5, which have $p/e < 5.0$, and $j/j_p > 2.26$. Because the three tubes have nearly the same j-factor, the deposition rate would be the same for all three tubes. The foulant removal rate is dependent on the shear stress. It is probable that the
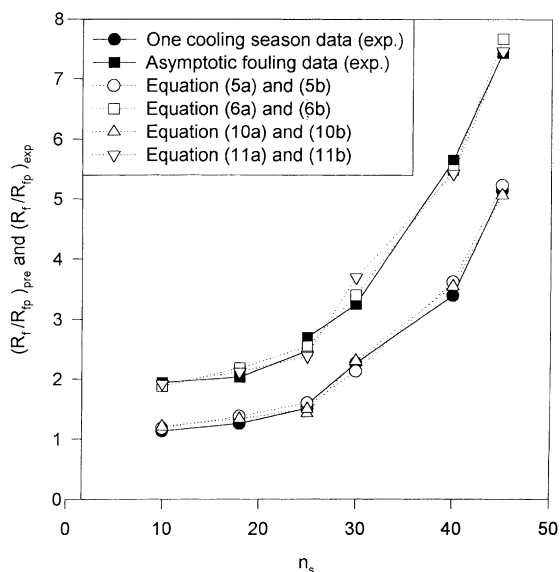
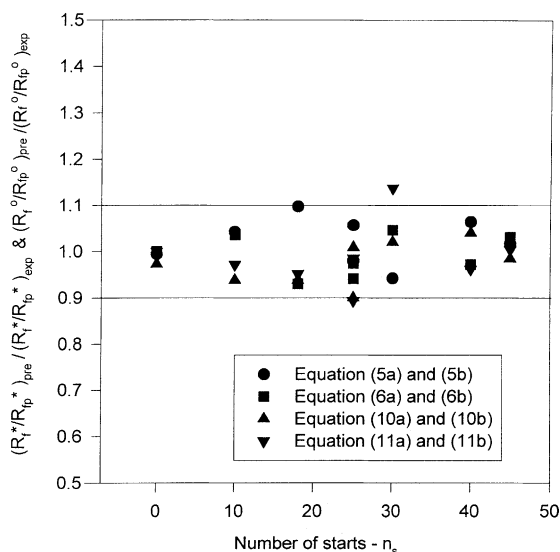Fig. 3. $(R_f/R_{fp})_{pre}$ and $(R_f/R_{fp})_{exp}$ vs. n_s.

Fig. 4. Error plot showing $(R_f^*/R_{fp}^*)_{pre}/(R_f^*/R_{fp}^*)_{exp}$ and $(R_f^\circ/R_{fp}^\circ)_{pre}/(R_f^\circ/R_{fp}^\circ)_{exp}$ vs. n_s.

small p/e ratio of these tubes results in a smaller actual shear stress than is assumed by Eq. (3). We believe this to be an important factor causing the high R_f^* ratio for tubes 2, 3, and 5. Further work is required to understand the physical nature of the flow and how it affects the removal process.

The key purpose of the correlations is to show the effect of the enhancement geometry on R_f for the low velocity operating conditions used. These correlations should not be used to infer what fouling results will exist

for higher water velocity or lower hardness. More data are required for such operating conditions.

4. Conclusions

1. A series of semi-theoretical fouling correlations as a function of $\beta\eta$ were developed. It is proposed that Eqs. (5a) and (5b), (6a) and (6b) are applicable to different internally ribbed geometries within the dimensional range of those tested. The correlations predicted the Table 1 fouling factors within 10%.
2. Eqs. (10a) and (10b), (11a) and (11b) can be used for similar commercial tube geometries correlations which have the following range of dimensions for any enhanced tube inside diameter: $0.024 \leqslant e/D \leqslant 0.041$, $2.81 \leqslant p/e \leqslant 9.88$, $25 \leqslant \alpha \leqslant 45°$, $\gamma = 41°$, $t_t/D_i = 0.015$. The correlations predicted the Table 1 fouling factors within 13%.
3. There are two ranges of fouling characteristics based on internal dimensions: a linear range and non-linear range. For tubes 6, 7, 8, 4, and plain tube, which $p/e \geqslant 5.0$, the R_f^* ratio linearly increases with increasing $\beta\eta$. For tubes 2, 3, and 5, which have $p/e < 5.0$, the linear relationship fails.
4. The correlations developed in this paper are for low water velocity – about half of the commonly used velocity for refrigerant condenser applications.

References

[1] X. Liu, M.K. Jensen, Numerical investigation of turbulent flow and heat transfer in internally finned tubes, J. Enhanced Heat Transfer 6 (1999) 105–119.
[2] R.W. Morse, J.G. Knudsen, Effect of alkalinity on the scaling of simulated cooling tower water, Can. J. Chem. Eng. 55 (1977) 272.
[3] J. Taborek, T. Aoki, R.B. Ritter, J.W. Palen, J.G. Knudsen, Fouling: the major unresolved problem in heat transfer, Chem. Eng. Progress 68 Part I (2) 59–67 (1972) and Part II (7) 69–78.
[4] N.-H. Kim, R.L. Webb, Particulate fouling of water in tubes having a two-dimensional roughness geometry, Int. J. Heat Mass Transfer 34 (11) (1991) 2727.
[5] E.F.C. Somerscales, A.F. Ponteduro, A.E. Bergles, Particulate fouling of heat transfer tubes enhanced on their inner surface, Fouling and Enhancement Interactions HTD-Vol. 164 (1991) 17.
[6] L.M. Chamra, R.L. Webb, Modeling liquid-side particulate fouling in enhanced tubes, Int. J. Heat Mass Transfer 37 (4) (1994) 571.
[7] A.P. Watkinson, Fouling of augmented heat transfer tubes, Heat Transfer Engineering 11 (3) (1990) 57.
[8] T.J. Rabas et al., Comparison of power-plant condenser cooling-water fouling rates for spirally indented and plain tubes, Heat Transfer Eng. 14 (4) (1993) 58.
[9] R.L. Webb, Principles of Enhanced Heat Transfer, Wiley/Interscience, New York, 1994 (Chapter 10).

[10] R.L. Webb, W. Li, Fouling in enhanced tubes using cooling tower water part I: long term fouling data, Int. J. Heat Mass Transfer 43 (2000) 3567.

[11] W. Li, A theoretical and experimental study of fouling in enhanced tubes in cooling tower systems, Ph.D. Thesis, Penn State University, 1998.

[12] W. Li, R.L. Webb, Fouling in enhanced tubes using cooling tower water part II: combined particulate and precipitation fouling, Int. J. Heat Mass Transfer 43 (2000) 3579.

[13] R.L. Webb, R. Narayanamurthy, P. Thors, Internal helical-rib roughness heat transfer and friction, J. Heat Transfer 122 (2000) 122–134.

[14] A.P. Watkinson, Interactions of enhancement and fouling, Fouling and Enhancement Interactions ASME HTD-Vol. 164 (1991) 1.

[15] S.H. Lee, Y.I. Cho, Velocity effect on electronic-antifouling technology to mitigate fouling in enhanced-tube heat exchanger, Int. J. Heat Mass Transfer, submitted.